J. Phys.: Condens. Matter 5 (1993) 1239–1256. Printed in the UK

Crystalline symmetry effects in x-ray magnetic circular dichroism in angle-resolved core-level photoemission

D Venus†, L Baumgarten‡, C M Schneider‡§, C Boeglin‡|| and J Kirschner‡§

† Physics Department and Institute for Materials Research, McMaster University, Hamilton, Ontario L8S 4M1, Canada

‡ Institut für Experimentalphysik, Freie Universität Berlin, D-1000 Berlin 33, Federal Republic of Germany

§ MPI für Mikrostrukturphysik, Halle/Saale, D-4050, Federal Republic of Germany¶

Received 13 November 1992

Abstract. The dependence of magnetic circular dichroism (MCD) in core-level photoemission on the experimental geometry and direction of electron emission has been studied experimentally using photoemission from the 2p and 3p levels of iron. The MCD has been measured both along emission directions of high symmetry, and along general emission directions within a single mirror plane. The observed angular variations cannot be accounted for by model calculations based on absorption, or based on angle-resolved emission into photoelectron states of a single, oriented atom. They are consistent with a model where the photoelectron states of the crystalline symmetry appropriate to couple to the detector are used.

1. Introduction

The study of magnetism using x-ray magnetic circular dichroism has evolved rapidly in experimental technique, areas of application, and in its interpretation. Erskine and Stern [1] originally proposed that the differences in the cross-section for the absorption of left- and right-circularly polarized soft x-rays would yield information about the polarization of the valence bands of itinerant magnets. In contrast, the first experiments were realized by van der Laan *et al* [2] as a method for studying localized ferrimagnetic moments, by using linearly polarized x-rays and measuring changes in the sample current as the sample was rotated. With the availability of circularly-polarized x-rays at some synchrotron facilities, Schütz *et al* [3] first applied the technique to itinerant magnets in a study of the 1s core level in iron. Later, as circularly polarized soft x-rays became available, Chen *et al* [4] measured x-ray MCD of the nickel 2p levels.

All of these results at absorption edges have been interpreted in terms of the magnetic exchange splitting of the valence states, with the addition of spin–orbit coupling in the valence states as required. Whereas Erskine and Stern [1] used a

|| Present address: Institut de Physique et Chimie des Materiaux de Strasbourg, Strasbourg Cédex, F-67070, France.

¶ This address is now permanent.

0953-8984/93/091239+18$07.50

on localized magnetic systems were more naturally explained using a model based on a single, oriented atom, which emphasized the role of the localized core hole [5, 6]. This approach was also necessary for a detailed understanding of the nickel spectra [7, 8]. Other metals, notably iron, appear to be amenable to the simpler, single-particle model. Ebert, Strange and Gyorffy [9] showed that a relativistic single-particle calculation is adequate for x-ray MCD from 1s core levels of iron, and Brouder and Hikam [10] also presented a single-particle formulation which included multiple scattering of the photoelectron. Carra *et al* [11] have used a hybrid model to understand MCD from gadolinium x-ray absorption edges, where single-particle states are used for the d valence bands and atomic orbitals for the 4f states. It is clear that both the atomic and single-particle approaches have strengths, depending on the features most prominently displayed by the system under study.

In the most recent evolution of x-ray MCD, Baumgarten *et al* [12, 13] measured the x-ray MCD in angle-resolved photoemission from the 2p and 3p core levels of iron. This phenomenon is qualitatively distinct from MCD in absorption, since the photoelectrons are in unbound states far above the Fermi level, and the effects of magnetic exchange splitting are seen at the core levels, not the valence levels. So long as the spin–orbit interaction separates the peaks sufficiently, this results in a characteristic plus/minus dichroic asymmetry within each peak of the core spectrum, as opposed to the asymmetry of a single sign for each peak, seen in absorption experiments. Still working within a calculation of the total (energy-resolved) absorption, Ebert *et al* [14] found that a single-particle model was adequate to describe the measurements on iron, and suggested that the core exchange splitting could be viewed as a ground-state property [15]. Van der Laan [16] and Thole and van der Laan [17] presented an atomic model, in which the core hole is coupled to the polarized valence electrons to produce the exchange splitting at the core, but did not compare the results directly to angle-resolved photoemission experiments. It has since become clear that, due to the angle-resolved nature of the experiment, neither of these approaches is adequate. Absorption is an integrated quantity which is rather insensitive to the details of the photoelectron state. Angle-resolved photoemission contains much more information about the wavefunction of the photoelectron. Thus Schneider, Venus and Kirschner [18] have shown that final-state selection gives rise to a more complicated experimental dependence of the x-ray MCD in photoemission than in absorption. They observed a strong dichroism in an experimental geometry where it would be forbidden by models based on absorption. It therefore appears that this recent variant of x-ray MCD offers new opportunities to test the understanding of both the core levels and the photoelectron states in MCD.

The purpose of the present paper is to substantiate and expand upon the angular selection effects of x-ray MCD in angle-resolved photoemission which have been reported briefly [18]. To this end, a more detailed description of both the experiments and the model for angular variation in the MCD are presented. New data confirm the origin of the angular variation, by ruling out other mechanisms. Further data investigate in detail emission in a general direction within a reflection symmetry plane. The model calculation, which was earlier applied only to emission along a high-symmetry direction (three or more reflection planes), is adapted to interpret the new data. This analysis demonstrates that it is not possible to understand the observed angular variation in the MCD using an oriented atom as a model. It is, however, consistent with the model when crystalline symmetry is included.

2. Experimental details

The experiments were performed on single-crystal iron samples. Each thin (1–2 mm) crystal was mounted across the poles of a C-shaped yoke of soft iron, so that it completed a magnetic circuit along an easy axis of magnetization. The sense of the magnetization was established by passing a current pulse through a wire wrapped around the yoke. The magnetic-domain structure of the samples was confirmed using the magneto-optic Kerr effect before mounting the sample holder in the vacuum chamber. The magnetizing current pulse was calibrated to give a single, remanent magnetic domain across the sample surface, with the exception of the extreme edges where it was attached to the yoke. All measurements were performed in remanence with the light striking a small, central portion of the sample. The yoke and a heating filament mounted behind the sample were surrounded by a molybdenum box. One face of the box was cut away to allow access to the crystal, and the edges of this opening were flush with the crystal face. This electrostatic shield, and the magnetic short circuit provided by the yoke, were effective in reducing stray fields such that their presence was not detected in the spectra. Stray magnetic fields might affect the MCD by deflecting the electron trajectories upon field reversal, and causing a false asymmetry. Absorption experiments are very sensitive to this artifact, since the MCD appears as a change in cross-section. Angle-resolved photoemission experiments are not as sensitive to stray magnetic fields, since the MCD asymmetry appears as a shift in peak energy. An artificial shift in the peak energies, or shapes, would appear with equal sign in the closely-spaced $2p_{3/2}$ and $2p_{1/2}$ peaks. Since these core levels show effective shifts of *opposite* sign in x-ray MCD in photoemission, the influence of stray magnetic fields is easily detected.

Two separate experimental runs were concluded at the BESSY synchrotron facility. The first used the SX-700-II monochromator [19] beamline, and an iron crystal with a (110) face. The x-rays provided by this monochromator are elliptically polarized, and can have a high degree of circularity if only a portion of the synchrotron beam is accepted, but it is not possible to reverse the sense of the ellipticity. Measurements of the beam position in the monochromator indicated that a large component of circularly polarized light with negative helicity is present. Although no quantitative measurements of the polarization were possible, an estimate based on previous calibrations and calculations [20] gives $P_c = 0.70 + 0.05/-0.10$ and $P_L = 0.71 + 0.10/-0.05$. The second experimental run used the SX-700-III monochromator beamline, and an iron crystal with a (001) face. This monochromator has optics which are very similar to those of the SX-700-II, so that the degree of circular polarization of the light is expected to be similar for a given angle above the synchrotron plane. It was possible to reverse the sense of the elliptically polarized light by moving the monochromator slit both above and below the synchrotron plane. In all cases, the dichroism was measured by reversal of the sample magnetization, not by reversal of the light helicity. Two interleaved photoelectron intensity spectra were accumulated for a given light helicity, with reversal of the sample magnetization between energy sweeps. This procedure avoids possible shifts in the energy scale (and thus false asymmetries) which might occur in repositioning the light beam on the monochromator as the light helicity is changed. In the second experimental run, the measurements were then repeated for light of the opposite helicity.

The experimental geometry is illustrated in figure 1. The coordinate axes $X'Y'Z'$ are aligned with the incoming light, such that Z' is along the wavevector q, and the

$Y'Z'$ plane is the plane of the synchrotron. The $X''Y''Z''$ coordinate axes are fixed to the crystal, with the sample magnetization along Z'', the surface normal along X'', and the crystal surface in the $Y''Z''$ plane. $Z''X''$ was a mirror symmetry plane of the crystal. The XYZ coordinate axes are oriented such that Z is along the direction of the electron emission, k, collected by the angle-resolving spherical-deflection energy analyser. The synchrotron beam and energy analyser are fixed, so that Y' is always parallel to Y, and the angle θ between the incident light and the emitted electrons was 135°. The angular degrees of freedom of the sample are specified by the angle β between the axes of magnetization and electron emission, and the angle α about the magnetization. $\alpha = 0$ corresponded to the crystal normal lying in the plane defined by q and k. The sample holder allows only one of these two angles to be varied for a given sample mounting geometry.

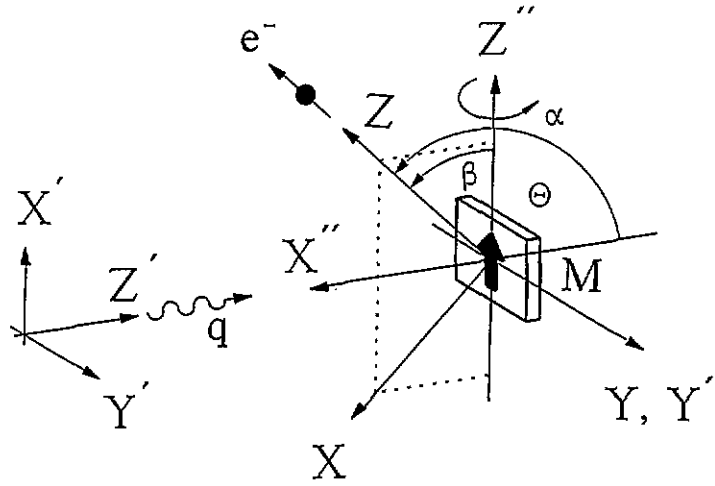

Figure 1. The coordinate systems used in the calculation. The coordinate system of the initial state, $X''Y''Z''$, is fixed to the crystal, with the polar axis determined by the direction of magnetization. The coordinate system of the dipole operator, $X'Y'Z'$, has its polar axis defined by the direction of light propagation. The coordinate system of the final state, XYZ, has its polar axis defined by the direction in which the photoelectrons are detected.

For the first experiments on Fe(110), a single spectrum has already been presented [18]. For this sample, β was fixed at 45° and α was varied between ±55°. Representative data are shown in figure 2. In figures 2(*a*) and 2(*b*) $\alpha = 0$, so that the light was normally incident, and the photoemission was collected in a mirror symmetry plane along a direction close to the ⟨111⟩ crystalline direction. A photon energy of 886 eV was used. The solid line in figure 2(*a*) is the sum of intensities for both magnetization directions as a function of photoelectron energy. The intensity asymmetry is plotted in figure 2(*b*), without any correction for background or the mixed polarization of the light. It is formed by subtracting the intensity spectrum for negative M from that for positive M, and dividing by their sum. Figure 2(*c*) shows the intensity asymmetry for data taken in the same geometry, but as a function of photon energy. Note that the energy scale runs from right to left to allow comparison to figure 2(*b*). The detected electrons had a kinetic energy of 188 eV above the

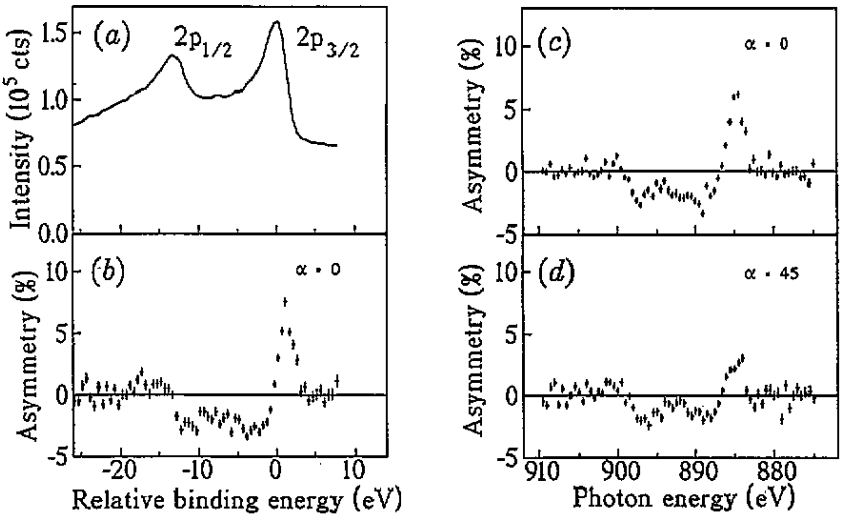

Figure 2. (*a*) The energy spectrum for photoexcitation of the $2p_{3/2}$ and $2p_{1/2}$ core levels of iron as a function of the photoelectron energy. The photon energy is 886 eV. The light is normally incident ($\alpha = 0$) on the (110) crystal face, and has wavevector q perpendicular to the sample magnetization M. Photoelectrons are collected at 45° to the surface normal, in the plane defined by q and M. The spectrum is the sum of two spectra taken with M in opposite directions. (*b*) The intensity asymmetry obtained by taking the difference of the spectra for $\pm M$ in part (*a*) and dividing by their sum. (*c*) As in part (*b*), except now the photoelectron energy is held constant and the photon energy is varied. Note that the scale runs from right to left. (*d*) As in part (*c*), except that the crystal is rotated by $\alpha = 45°$ about the direction of magnetization, so that the light is no longer normally incident on the crystal surface.

Fermi level. In figure 2(*d*), the intensity asymmetry of data collected with $\alpha = 45°$ with respect to the mirror plane is again plotted as a function of the photon energy.

The general shape of the asymmetry curves in figure 2 can be understood qualitatively using the independent-electron model [14]. An equivalent argument can be made using an atomic model [16]. In magnetic circular dichroism in core-level photoemission, the principal effects of both spin–orbit coupling and the magnetic exchange field are in the core-level states. The spin–orbit coupling makes $2p_{3/2}$ and $2p_{1/2}$ initial states. The magnetization splits these states energetically according to the projection of the angular momentum, m_j, onto the field axis [15]. Thus, states with m_j in a field $+M$, and states with $-m_j$ in a field $-M$, have the same energy. The intensity of the photoexcitation from these states also depends on m_j, because of the dipole selection rules for circularly polarized light. Transitions from the states with m_j and $-m_j$ therefore have different intensities but occur at the same energy in the photoelectron spectrum when the magnetization is reversed. This creates an intensity asymmetry. At the photoelectron energy corresponding to excitations from initial states $-m_j(+M)$ and $m_j(-M)$ there is an essentially equal, but opposite, intensity asymmetry producing the plus/minus features characteristic of dichroism in photoemission. Because the $2p_{1/2}$ and $2p_{3/2}$ states have opposite senses of spin and orbital alignment ($l - s$ versus $l + s$), the sign of the energy splitting for a given $m_j(M)$ is reversed in the two peaks. The dipole selection rules, however, are unchanged, so that if a plus/minus asymmetry occurs at the $2p_{3/2}$ peak, a minus/plus

feature occurs in the dichroism at the $2p_{1/2}$ peak. All of these features are clear in figure 2.

The striking occurrence reported briefly earlier [18], is that the asymmetry in, for example, figures 2(*b*) and 2(*c*), is non-zero when the light is normally incident. In fact it is roughly 1.5 times larger than has been previously observed at glancing light incidence [12, 13]. Since MCD requires the circularly polarized light to act on states of different m_j, but with the same energy in a magnetized sample, the effect was expected to disappear unless some component of the helicity (or, equivalently, the unit vector $\hat{q}$) is along the unit vector parallel to the magnetization axis, $\hat{M}$ [12, 14, 16],

$$\hat{q} \cdot \hat{M} \neq 0. \tag{1}$$

This condition is, of course, also required for the magnetic circular dichroism effects at the absorption edges [9, 10, 21]. Important additional data which shed light on the apparent contradiction of equation (1) are presented in figures 3–5.

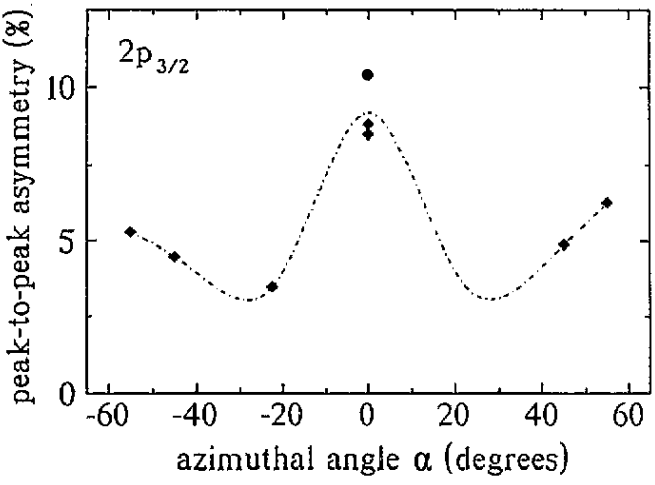

Figure 3. Variation of the peak-to-peak dichroic asymmetry at the $2p_{3/2}$ feature as a function of the angle α. The geometry is as before, with $\hat{q} \cdot \hat{M} = 0$, and photoelectrons collected at 45° from both q and M ($\beta = 45°$). The line is a guide to the eye. The sample is Fe(110).

As can be seen in figure 2(*d*), when the crystal is rotated about the magnetization by angle α (so that the relative alignment of q and M does not change), the magnitude of the dichroic asymmetry changes. The peak-to-peak asymmetry at the $2p_{3/2}$ peak is plotted in figure 3 for a few angles α about the crystalline mirror plane. The symbols represent individual measurements of high precision, but the magnitude of the observed asymmetry depends on the secondary-electron background in the spectrum (for which no correction is made). The reproducibility of the data is best judged from the points at $\alpha = 0$, which result from independent spectra collected on different days. An important point is that the *sign* of the asymmetry does not change in passing through the mirror plane ($\alpha = 0$). Rather, the peak-to-peak amplitude is a symmetric function of α. This rules out the possibility that the asymmetry is due to the transmission of the photoelectrons at the surface of the crystal. Because of the spin–orbit splitting in the $2p_{1/2}$ and $2p_{3/2}$ initial electronic states, the use of circularly polarized light leads to spin-polarized photoelectrons. This spin polarization might be transformed into an intensity asymmetry by spin-dependent surface transmission

due to the effects of spin–orbit coupling in the photoelectron states [22]. However, this mechanism creates an intensity asymmetry only when the emission direction is not in a spatial mirror plane, and the asymmetry must reverse its sign on opposite sides of the plane [23]. This contradicts figure 3. Furthermore, if surface transmission effects were important, the shape and sign of the dichroic asymmetry should be very sensitive to the emission geometry and energy changes on a scale of ~ 2 eV [22]. This is clearly not the case, since the asymmetry curve taken by varying the final-state energy (figure 2(*a*)) is essentially identical to that obtained at a constant final state energy (figure 2(*b*)). Data taken at other photon energies (850, 900, 950 eV: see section 4) show the same form of asymmetry curve as in figure 2, but with varying magnitudes of asymmetry. Thus the phenomenon does not depend on explicit details of the final states for its existence.

A second important observation is presented in figure 4. This shows the magnetic circular dichroism of the 3p levels of iron, once again measured with light normally incident ($\alpha = 0$) on the (110) surface, with $\hat{q} \cdot \hat{M} = 0$, $\theta = 135°$, $\beta = 45°$. A photon energy of 233.5 eV was used. The 3p levels are qualitatively different than the 2p levels, since the exchange splitting is larger and can no longer be treated as a perturbation of the spin–orbit coupling. However, the magnetic circular dichroism persists, and the peak-to-peak asymmetry is again ~ 1.5 times larger than in the previous experiments studying the iron 3p levels at glancing light incidence [13]. This suggests that the persistence of the dichroism at $q \cdot M = 0$ is a general phenomenon which does not depend on the explicit details of the initial core states.

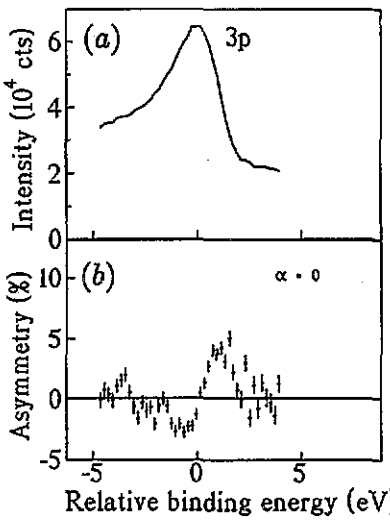

Figure 4. The intensity, (*a*), and dichroic asymmetry, (*b*), of the photoemission from the 3p core levels of iron, as functions of the binding energy. The photon energy is 223.5 eV. The geometry is as before, with $\hat{q} \cdot \hat{M} = 0$, $\alpha = 0$, and $\beta = 45°$. The sample is Fe(110).

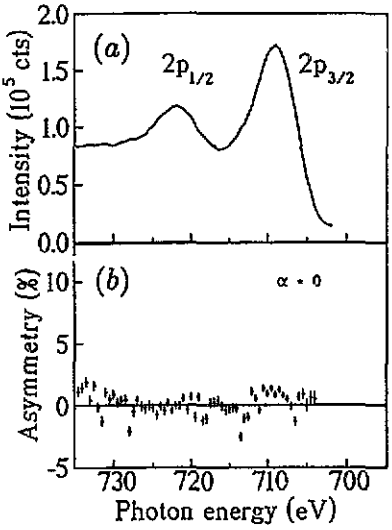

Figure 5. The intensity, (*a*), and dichroic asymmetry, (*b*), of the $L_3M_{23}M_{23}$ Auger electrons as the photon energy is varied. The geometry is as before, with $\alpha = 0$ and $\beta = 45°$. The sample is Fe(110).

Finally, it is important to make connection with the absorption experiments where equation (1) does hold. This may be done by collecting angle-resolved

Auger electrons instead of photoelectrons. Auger electron emission within a small solid angle comprises contributions involving photoexcitation into all the accessible photoelectron states. Although the contributions associated with each photoelectron state may not be equal, the angle-resolved Auger emission is to a great extent a measure of the angle-integrated photoemission. It is therefore expected that the Auger electrons show no dichroic asymmetry when $q \cdot M = 0$, in agreement with the predictions of an absorption experiment. Figure 5(*a*) shows the intensity of the $L_3M_{23}M_{23}$ Auger electrons from iron as a function of photon energy, as the photon energy is swept through the 2p absorption edges. The data were collected in the same geometry ($q \cdot M = 0$, $\alpha = 0$ and $\beta = 45°$) and with the same angle-resolving spectrometer as the other data. The intensity asymmetry which results from reversal of the magnetization direction is shown in figure 5(*b*). There is some scatter in the data points, which (other than a few outlying single points) is confined to absolute asymmetries $\leqslant 1.5\%$. Comparison with figure 2(*a*) shows that the ratio of the secondary-electron background to the $2p_{3/2}$ peak in the Auger electron spectrum, is at least a factor of four smaller than the same ratio in the photoelectron spectrum. If the two spectra had the same background/signal ratio, the range of asymmetries in the Auger spectrum would be reduced to about $\leqslant 0.4\%$, which is a null result indistinguishable from the noise in the photoelectron spectra [24]. In summary, figure 5 shows no MCD at a level of the noise in the photoemission spectra. The importance of this result is two-fold. First, by using the identical measurement geometry, it demonstrates that the dichroism observed in photoemission is not the result of an experimental artifact, such as stray magnetic fields [25]. Second, it confirms that, when $q \cdot M = 0$, one may simultaneously observe a large MCD in angle-resolved photoemission, and no MCD in absorption. Therefore, the photoemission results do not contradict previous angle-integrated theoretical and experimental results.

These considerations make it clear that the observed asymmetries are truly MCD in core-level photoemission, despite the predictions that it should vanish in this experimental geometry. With these data in hand, it is now possible to formulate an explanation for the angular dependence of the MCD in photoemission based on general principles of angle-resolved photoemission.

3. Model of angular selection effects

The data suggest that the origin of the contradiction with the earlier calculations is found in the difference between an absorption experiment and angle-resolved photoemission. Since only photoelectrons emitted in a certain direction are detected, more attention must be given to specifying the angular variation of the photoelectron wavefunction. The angular selection effects are most properly taken into account in a 'one-step' photoemission calculation using either time-reversed LEED (low-energy electron diffraction) states, or states where the effects of photoelectron diffraction are included. However, as the previous discussion has demonstrated that the observed asymmetries cannot arise from surface transmission, the important points are already present in the 'three-step' model of photoemission. The central observation is that in the photoexcitation matrix elements

$$M_{fi} = \langle \Psi_f(\Omega) | O_h(\Omega') | \Psi_i(\Omega'') \rangle \delta(E_f - h\nu - E_i) \tag{2}$$

the co-ordinate systems (denoted by the different solid angles Ω, Ω', and Ω'') in which the dipole operator O_h and wavefunctions Ψ are naturally expressed, are different. These co-ordinate systems are illustrated in figure 1.

Because the angular dependence is expected to arise from effects of the photoelectron states, and because it has proved adequate in previous treatments of MCD in iron [9, 14], a simple independent-electron expression for the core states is used. Given the strong spin–orbit coupling in the localized initial 2p states, $\Psi_i(\Omega'')$ can be represented by perturbed $2p_{1/2}$ or $2p_{3/2}$ atomic states. The angular variation of the unperturbed spin–orbit split atomic states $R_\kappa^\mu(r'')\chi_\kappa^\mu(\Omega'')$ is given by [26]

$$\chi_\kappa^\mu(\Omega'') = \sum_{m''} C(1, \tfrac{1}{2}, j; m'', \mu - m'')Y_{1,m''}(\Omega'')|\mu - m''\rangle. \tag{3}$$

Here κ indicates the values of both l and j. $\kappa = 1$ for the $p_{1/2}$ state and $\kappa = -2$ for the $p_{3/2}$ state, and μ is the azimuthal quantum number m_j. $|\mu - m''\rangle$ is a Pauli spinor $|\sigma''\rangle$. The $C(j_1 j_2 j; m_1 m_2)$ are the Clebsch–Gordan coefficients.

In the independent-electron approach [14], the ferromagnetic alignment of both the valence and core electrons is considered a ground-state property. The magnetization lifts the degeneracy of the core sublevels with different μ, and introduces a small mixing between the $2p_{1/2}$ and $2p_{3/2}$ states with identical values of μ. For the 2p states, the resultant exchange splitting is much smaller than the spin–orbit splitting, and the mixing can be treated as a first-order perturbation [14, 15]. To first order, the radial part of the wavefunctions, R_κ^μ, for $\pm\mu$ now differ slightly, but in such a way that $R_\kappa^\mu(M) = R_\kappa^{-\mu}(-M)$. This can affect the total intensity of the photoemission peak, but not the dichroic asymmetry, and is therefore of secondary importance. The angular part of the wavefunction, $\chi_\kappa^\mu(\Omega'')$, is unchanged, but the magnetization defines a specific orientation of its polar axis. The Pauli spinor has its axis of quantization along the sample magnetization (with a positive sense coinciding with a negative sense of magnetization), and the spherical harmonic has its polar axis along Z'' (parallel or anti-parallel to M, depending on κ, i.e. depending on whether $j = l + s$ or $l - s$). The energy of the core sublevels is perturbed in first order by an exchange splitting, $2\mu\epsilon$, proportional to μ and M [15].

The dipole operator $O_h(\Omega')$ for circularly polarized light of helicity $h = m'$ is represented by the spherical harmonic [26] $-m'Y_{1,m'}(\Omega')$, where the polar axis is along Z', parallel to q. For the final states $\Psi_f(\Omega)$ in the three-step model, effects due to spin–orbit coupling and exchange splitting are neglected, as they are not essential to the existence of the magnetic dichroism. Band states are used, since LEED shows that electrons 100–200 eV above the Fermi energy continue to feel the influence of the lattice potential and symmetry [27]. The states are expressed with their polar axis along the emission direction, Z. This is because it is the symmetry operations with respect to the emission direction which determine which wavefunctions are coupled to the planewave states at the detector. That portion of each band state which transforms as the totally symmetric group representation has the correct symmetry to couple to the detector [28]. Only this portion is included in the calculation. Thus, the 'symmetry projected' d-like final states have an angular variation described by some mixture of spherical harmonics

$$\Psi_f(\Omega) = \sum_m B_m(\alpha, \beta)Y_{2,m}(\Omega)|\sigma\rangle \tag{4}$$

where the expansion coefficients $B_m(\alpha,\beta)$ depend on the orientation of the emission direction k with respect to the crystal through the angles α and β. These coefficients could, in principle, be calculated within a one-step or three-step model of photoemission, but their explicit calculation is not of primary interest here. Rather, it is the fact that symmetry requires some of the $B_m(\alpha,\beta)$ to be zero along some emission directions which is relevant.

The changes in the matrix element due to the radial part of the wavefunction are expected to be small and regular, and are cancelled to a great extent in forming the intensity asymmetry. They are therefore neglected. This results in a series of matrix elements of the angular wavefunctions of the form

$$M_{if} = \sum_m B_m^*(\alpha,\beta) \sum_{m''} C(1,\tfrac{1}{2},j;m'',\mu-m'') M^{m'}_{m,m''}(\sigma|\mu-m'') \tag{5}$$

where

$$M^{m'}_{m,m''} = \langle Y_{2,m}(\Omega)|Y_{1,m'}(\Omega')|Y_{1,m''}(\Omega'')\rangle \tag{6a}$$

$$= \sum_{\mu'} D^1_{\mu',m'}(\alpha'\beta'\gamma') \sum_{\mu''} D^1_{\mu'',m''}(\alpha''\beta''\gamma'')\langle Y_{2,m}(\Omega)|Y_{1,\mu'}(\Omega)|Y_{1,\mu''}(\Omega)\rangle. \tag{6b}$$

The transformation matrices $D^1_{\mu,m}(\alpha,\beta,\gamma)$ have been used to express all quantities in terms of the final state reference frame, where α, β, and γ are the Euler angles required to rotate from one reference frame to another [26]. Reference to figure 1 shows that for the dipole operator $\alpha' = \gamma' = 0$, $\beta' = \theta$, and for the initial states, $\alpha'' = -\alpha$, $\beta'' = \beta$, and $\gamma'' = 0$. The matrix elements in equation (6*b*) can be evaluated using Clebsch–Gordan coefficients [26]. The square modulus of the matrix element M_{if} in equation (5) is evaluated for angles β and $\beta+\pi$ to represent a reversal of magnetization, and the (μ,κ)-resolved (i.e. energy-resolved) intensity asymmetry is calculated.

For the case of emission in a single mirror plane of the crystal, the totally symmetric representation contains the even d-like combinations: $Y_{2,0}$, $1/\sqrt{2}\,(Y_{2,1} - Y_{2,-1})$ and $1/\sqrt{2}\,(Y_{2,2}+Y_{2,-2})$. A relatively simple closed expression can be given for the maximum possible dichroic asymmetry of the $2p_{1/2}$ peak using just the transition strengths. This is equivalent to assuming no lifetime broadening or instrumental broadening. The dichroic asymmetry $A^{m'}_{1m}(\mu,\kappa)$ in the $2p_{1/2}$ peak ($\mu = \pm\frac{1}{2}$, $\kappa = 1$), when light of negative helicity is incident ($m' = -1$), considering all d-like final states ($l = 2$) of even symmetry ($m \equiv e$), is

$$A^{-1}_{2,e}(\mu,1) = \mathrm{sgn}(\mu)\frac{a\cos(\theta-\beta) - 2b\cos\theta\cos\beta + c\sin(\theta+\beta)}{d + b\sin^2\theta + c\sin\theta\cos\theta} \tag{7}$$

where

$$a = 4|B_0|^2 + 4\sqrt{3}\,\mathrm{Re}[B_0 B^*_{2e}] \qquad b = 3|B_0|^2 - 3|B_{2e}|^2 + 2\sqrt{3}\,\mathrm{Re}[B_0 B^*_{2e}]$$
$$c = 2\sqrt{3}\,\mathrm{Re}[(B_0 + B_{2e})B^*_{1e}] \qquad d = 2|B_0|^2 + 6|B_{2e}|^2 + 3|B_{1e}|^2$$

and where the expansion coefficients B_m are understood to depend on α and β. The effect of applying a total broadening Γ to the δ-function transitions is to reduce the

magnitude of the asymmetry, according to a function of the exchange splitting and Γ. Broadening does not, however, affect the ratio of the predicted asymmetry for different geometries.

The dichroic asymmetry of the $2p_{3/2}$ peak is more complicated, since it contains more than a single $|\mu|$. The ratios of the asymmetries in different geometries now depend slightly on the exchange splitting and Γ. Although the calculation is straightforward, a simple, closed expression such as equation (7) is not possible, except in the extreme limit of poor energy resolution (small ϵ/Γ). The effect of poor energy resolution is to group the $\mu = +\frac{3}{2}$ and $+\frac{1}{2}$ contributions together, so that the asymmetry between this pair of levels and the pair $\mu = -\frac{3}{2}$ and $-\frac{1}{2}$ is what is seen experimentally. For the totally symmetric representation discussed above, this pairing produces an expression for the dichroic asymmetry which is identical to equation (7), with an additional negative sign. The finite energy resolution also reduces the overall magnitude of the asymmetry. For 2p iron core levels, $\epsilon \approx 0.2$ eV [15,29] and, in the present experiments, $\Gamma = 2.0$ eV HWHM. Convolution of the transition lines with a Lorentzian shows that these parameters are within the limit of small ϵ/Γ discussed above. Thus, equation (7) applies equally to the dichroic asymmetry at the $2p_{3/2}$ peak, so long as a negative sign is included, and a constant scaling factor resulting from the energy resolution is calculated.

The model results are consistent with the data presented in section 2. Most fundamentally, the dichroic asymmetry is a minus/plus feature (because of the factor of $\mathrm{sgn}(\mu)$), and reverses sign when the light helicity is reversed. The latter can be demonstrated by recalling that reversing the polarization of circularly polarized light is equivalent to reversing the direction of propagation, $\hat{q}$, while maintaining the sense of rotation of the electric vector. This is simulated by allowing θ to become $\theta + \pi$ in the calculation, and all the asymmetries change sign. Similarly, if both the magnetization and light helicity are reversed ($\theta \rightarrow \theta + \pi$ and $\beta \rightarrow \beta + \pi$), the asymmetry is unchanged. It is also evident that the angle-resolved asymmetry persists at $\cos(\theta - \beta) = \hat{q} \cdot \hat{M} = 0$, since other non-zero terms remain in the numerator. Various high-symmetry limits are also contained in equation (7). For emission along a line containing two mirror planes [30], $B_{1e} \equiv 0$, so that $c = 0$. Then the numerator contains only terms varying like $\hat{q} \cdot \hat{M}$ and $\cos\theta \cos\beta = (\hat{q} \cdot \hat{z})(\hat{z} \cdot \hat{M})$. For emission along a direction containing three or more mirror planes, $B_{2e} = 0$ as well [30], and equation (7) reduces to that presented earlier [18] for emission along a [111] direction. In this case, the one remaining expansion coefficient cancels from the numerator and denominator, and quantitative comparisons of different geometries can be made [18].

For emission along a general direction, the odd combinations of the $Y_{2,m}$ must also be included. The expression analogous to equation (7) is more complicated, and there is little merit in producing it here. However, like equation (7), it depends on α only through the expansion coefficients, since none of k, q, or M change as α is varied. Since the expansion coefficients are the same for two directions $\pm\alpha$ related by reflection in a mirror plane, the dichroic asymmetry also shows mirror symmetry, as in figure 3.

Finally, consider an absorption experiment performed at an absorption edge. In this case, the photoelectrons do not escape and an angle-integrated measure of absorption is used. It is no longer correct to restrict the calculation to only that portion of the final band states which couples to the detector. Rather, absorption by an entire d band is equivalent to absorption by an entire atomic d multiplet. Each

$Y_{2,m}$ should therefore be weighted equally, and no interference terms occur. Then all terms such as $(\hat{q}\cdot\hat{z})(\hat{z}\cdot\hat{M})$ sum to zero, and equation (1) is recovered,

$$A_{2,c}^{-1}(\mu,1) = \mathrm{sgn}(\mu)\tfrac{1}{2}(\hat{q}\cdot\hat{M}) \tag{8}$$

where $m \equiv c$ stands for a complete multiplet. This is in agreement with the Auger data in figure 5, where $q\cdot M = 0$. Similarly, emission into s-like final states ($l = 0$), shows spherical symmetry even in an angle-resolved experiment. For s-like final states,

$$A_{0,0}^{-1}(\mu,1) = A_{0,c}^{-1}(\mu,1) = -\mathrm{sgn}(\mu)(\hat{q}\cdot\hat{M}). \tag{9}$$

Thus the dichroism in photoelectrons excited from 2p levels to s- and d-like final states is simply related by a factor of -2 in angle-integrated photoemission (as has been pointed out by Imada and Jo [31]), but are not simply related in angle-resolved photoemission.

An experimental investigation of the dependence of equation (7) on β is the subject of section 4. Other predictions based on this model are not amenable to experimental verification in the present geometry of the apparatus. Although there is no general geometry in the mirror plane which will give zero dichroic asymmetry, the model does predict a null geometry for emission along higher symmetry directions (when at least $B_{1e} = 0$). In figure 1, this occurs when $\theta = \pi/2$, $\beta = 0$ or when $\theta = 0$, $\beta = \pi/2$ (and multiples of π). Since the magnetization at the surface of a bulk crystal of iron lies in the crystal surface, these geometries involve extreme grazing light incidence or electron emission and are difficult to realize. Another possibility is when $\hat{M}$ is along the Y'' axis in figure 1, and $\alpha = 0$. In this case the dichroism disappears independent of the values of θ and β. This experiment has not yet been attempted, since it would require a rebuilding of the sample holder.

4. Dependence on crystal orientation

The crystallographic directional dependence of MCD in angle-resolved photoemission is contained in the expansion coefficients $B_m(\alpha,\beta)$ for a certain emission direction k. Previous work [18] has concentrated on emission along the high-symmetry [111] direction, where only B_0 is non-zero, and the dichroic asymmetry is independent of B_0. Although a modulation of the magnitude of the dichroic asymmetry consistent with changes in emission geometry was observed, it is not clear that this was a crystalline effect. Suppose that the system under study was modelled as a single, oriented atom instead of as a crystal. Such a model, using atomic final states, has wide application in angle-integrating absorption experiments, and is suggested for MCD in photoemission as well [16]. Since the atom has spherical symmetry, only those states transforming as $Y_{l,0}(\Omega)$ would couple to the plane wave at the detector [32]. For d-like final states only the $Y_{2,0}(\Omega)$ term is non-zero and the expression for the dichroic asymmetry is identical to that for emission along a crystalline direction of high symmetry. It is possible to test for crystalline effects only by moving to an emission direction of lower symmetry, such as within a single mirror plane. Then equation (7) indicates that, for crystalline final states, more expansion coefficients become important. A model using final states of a single atom does not show these changes, since only $Y_{2,0}$ is coupled to the detector in any emission geometry. In the absence

of detailed calculations of the B_m, it is still possible to detect crystalline symmetry (and possibly other) effects as deviations of the measured dichroic asymmetry from the limiting case of an oriented atom. It may be that the nature of the deviations will indicate whether or not they are due to the crystalline symmetry of the final states.

These ideas were tested in the second experimental run, using a (001)-oriented single crystal of iron and the SX-700-III monochromator at BESSY. The sample was mounted such that the angle β could be varied, but α was fixed at $\alpha = 0$, a mirror plane containing the crystal normal. Once again, $\theta = 135°$. Photoelectron spectra of emission from the 2p core levels were recorded as functions of the kinetic energy of the photoelectrons for photon energies of 850, 900 and 950 eV, over a range of $35° < \beta < 125°$. The dichroic asymmetry upon reversal of the magnetization was found, and the experiments were repeated for light of opposite helicity.

A representative pair of spectra for $\beta = 120°$ are presented in figure 6. The dichroic asymmetry curves show the expected reversal of sign upon change of light helicity. The peak-to-peak asymmetry at the $2p_{3/2}$ and $2p_{1/2}$ features are plotted as a function of β in figure 7. In order to remove systematic and apparatus asymmetries, the peak-to-peak dichroic asymmetry was evaluated as one half the difference of the peak-to-peak asymmetries of the separate measurements with each sense of light helicity. Data points for all three photon energies are plotted together, since no significant variation with photon energy was observed. No correction was made for the secondary-electron background, or for the incomplete circular polarization of the light. The lines in figure 7 are the model prediction for the peak-to-peak dichroic asymmetry in emission from the 2p states into states of $Y_{2,0}(\Omega)$ symmetry only, as would be appropriate for an oriented atom.

The calculated curves in figure 7 have been normalized to the $2p_{3/2}$ data at $\beta = 90°$, since this angle represents normal emission along the high-symmetry [001] direction, and emission only to states of $Y_{2,0}(\Omega)$ symmetry is appropriate even in crystals. As such, it is possible to make a quantitative comparison between this geometry and previous results along high-symmetry directions [12, 18]. The data in figure 7 show a peak-to-peak asymmetry of 0.086 ± 0.005. This value is compared to the previous experiments and the model calculation (with energy broadening included) in table 1. The model properly predicts the sign and relative magnitude of the dichroic asymmetry in very different geometries, and gives an excellent account of relative variations with experimental geometry. This confirms that the final state selection effects described by the model are very important in an angle-resolved experiment.

To test whether or not the model yields a reasonable quantitative value for the dichroic asymmetry along a high-symmetry direction of emission, it is necessary to allow for the elliptical polarization or the light, and for the secondary electron background. Letting $m' \equiv$ e or c for elliptically or circularly polarized light, the asymmetry in emission from the $2p_{1/2}$ level to final states of symmetry $Y_{2,0}$ is

$$A^{e}_{2,0}(\mu, 1) = A^{c}_{2,0}(\mu, 1) P_C [1 + P_L 3\sin^2\theta/(2 + 3\sin^2\theta) + B/S]^{-1}. \quad (10)$$

P_C and P_L are the degree of circular and linear polarization [33], and B/S is the ratio of the secondary-electron background to the total signal. The geometric factor multiplying P_L has a different form for other final-state combinations. Since the experiment was performed in the limit of poor energy resolution, this expression is also valid for the $2p_{3/2}$ asymmetry. If the background is estimated roughly as the mean of the count rates on either side of the $2p_{3/2}$ peak, the calculated asymmetry in

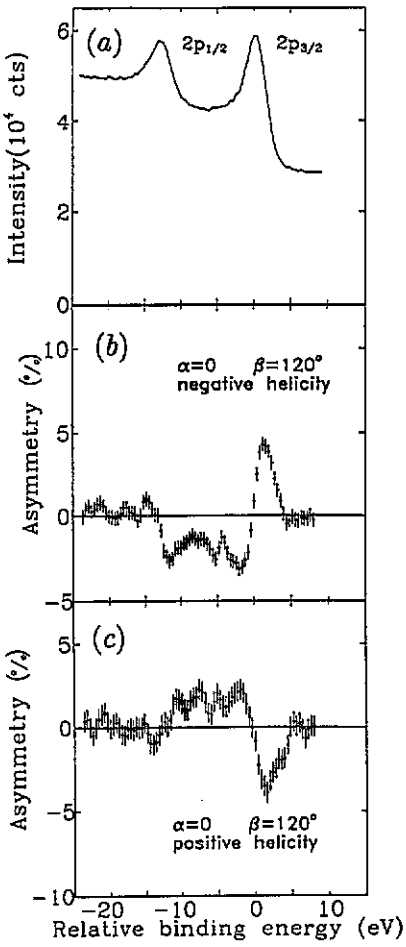

Figure 6. Intensity, (*a*), and dichroic asymmetry, (*b*) and (*c*), of the photoemission from the 2p core levels of iron, for emission within a single mirror plane, with $\theta = 135°$, $\alpha = 0°$ and $\beta = 120°$. In parts (*a*) and (*b*), light of negative helicity is used. In part (*c*), light of positive helicity is used. The photon energy is 900 eV, and the sample is Fe(001).

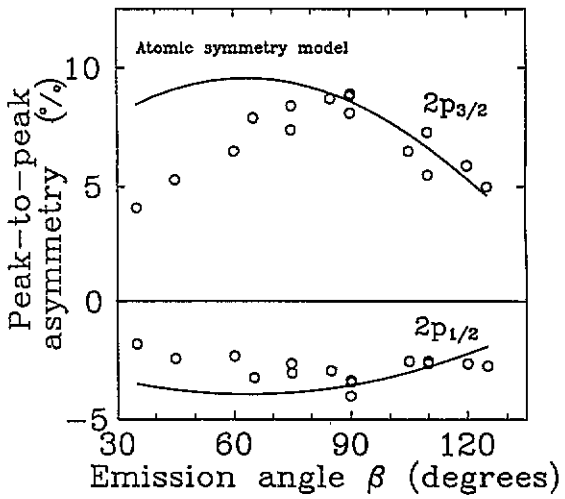

Figure 7. The peak-to-peak dichroic asymmetry at the $2p_{3/2}$ and $2p_{1/2}$ features are plotted as functions of the angle β. The lines are the result of the model calculation for final states of $Y_{2,0}(\Omega)$ symmetry, which have been normalized to the $2p_{3/2}$ data at $\beta = 90°$. The exchange splitting parameter $\epsilon = 0.2$ eV, and the energy resolution is $\Gamma = 2.0$ eV HWHM. The geometry is as before, with $\alpha = 0$. The sample is Fe(100).

column 3 of table 1 must be reduced by a factor of $0.38 + 0.03/ - 0.06$. This leaves roughly a consistent discrepancy of a factor of two between the model calculation and experiment. Given the simplicity of the model, better absolute agreement is not expected.

Returning to the $2p_{3/2}$ data for emission from within a mirror plane (figure 7), there is a clear angular variation in the magnitude of the dichroic asymmetry. This is not an experimental artifact. It is not due to sampling regions near the edge of the crystal as the angle is varied, since the x-ray beam strikes only a small, central portion of the crystal face. It is not due to sampling different magnetic domains as the angle is varied, since the magneto-optic Kerr effect has been used to confirm that there is

Table 1. Comparison of the observed and calculated peak-to-peak asymmetries in magnetic circular dichroism for different geometries.

	Reference [12]	Present work (β fixed)	Present work (α fixed)
Surface	Fe(110)	Fe(110)	Fe(100)
Emission	$\approx$ [111]	$\approx$ [111]	[100]
β	55°	45°	90°
θ	65°	135°	135°
Expt. $A(2p_{3/2})$			
absolute	0.040[a]	0.092±0.010	0.086±0.005
relative	0.44	1.00±0.11	0.94±0.05
Model $A(2p_{3/2})$[b]			
absolute	0.194	0.415	0.392
relative	0.467	1.000	0.945
Expt. ratio $A(2p_{1/2})/A(2p_{3/2})$	−0.36[a]	-0.37 ± 0.05	-0.42 ± 0.05
Model ratio[b] $A(2p_{1/2})/A(2p_{3/2})$	−0.40	−0.41	−0.41

[a] Single measurement at poorer energy resolution.
[b] Exchange splitting $\epsilon = 2\mu$ (0.2) eV and line broadening $\Gamma = 2.8$ eV HWHM (column 1) and 2.0 eV (columns 2 and 3).

a single, large magnetic domain in the central portion of the crystal face which is locked in place by a permanent magnet. It is not due to a change in the energy resolution of the spectra as the angle is varied. It is not due to the presence of a component of linearly polarized light, since equation (10) shows that this introduces a dependence on θ, but not on β. It is not due to changes in the relative size of the secondary electron background as the angle is varied. The secondary-electron background does depend slightly on β, but introduces a correction which is an order of magnitude too small to account for the experimental curve. Finally, it is not due to variations in the escape depth of the photoelectrons as the angle is varied. This would have no effect for a crystal which is magnetized uniformly as a function of depth. A simple calculation assuming an escape depth given by the 'universal curve' shows that a magnetically dead layer 7 ML thick would be required to simulate the experimental results. Iron single-crystal surfaces, even if contaminated by trace amounts of carbon, do not have magnetically dead layers, especially not of such thickness [34].

The variation in the magnitude of the asymmetry at the $2p_{3/2}$ peak is not well described by the model applied to an oriented atom (line in figure 7). The data shows a maximum asymmetry at $\beta = 90°$ (compare $\beta = 65°$ in the calculation), and a much faster variation with β than the calculation. That both of these discrepancies are consistent with crystalline effects can be inferred from equation (7). The asymmetry depends on β explicitly, and implicitly through the expansion coefficients $B_m(\alpha = 0, \beta)$. Since the direction ($\alpha = 0$, $\beta = 90°$) is along [001], it lies in a second, orthogonal mirror plane, and $B_m(\alpha = 0, \beta = 90° + \delta) = B_m(\alpha = 0, \beta = 90° - \delta)$. If the crystalline effects are of overriding importance, this implicit dependence on β will cause the dichroic asymmetry to have mirror reflection about $\beta = 90°$. This is in agreement with figure 7. The general shape of the curve can also be

inferred from equation (7). The maximum occurs at $\beta = 90°$, for emission along a high-symmetry direction where only B_0 is non-zero. Moving away from $\beta = 90°$ allows inclusion of final states transforming as $(Y_{2,1} - Y_{2,-1})\sqrt{2}$ through B_{1e}, and $(Y_{2,2} + Y_{2,-2})\sqrt{2}$ through B_{2e}. There are both diagonal (modulus-squared) and off-diagonal (interference) contributions. The diagonal term in B_{1e} gives zero asymmetry, and the diagonal term in B_{2e} gives a contribution of sign opposite to that for B_0. These both serve to reduce the dichroic asymmetry and are expected to have a larger influence as β departs more from 90°. It is not possible to be conclusive about the interference terms. However, since the relative phases of B_0, B_{1e}, and B_{2e} are expected to be randomly distributed, they will tend to give neither a positive nor a negative contribution to the dichroic asymmetry, but rather to 'dilute' it. In summary, the peak position, mirror symmetry and negative curvature (near $\beta = 90°$) of the angular dependence of the dichroic asymmetry, all indicate the presence of crystalline, and not atomic, final-state symmetry. Quantitative calculations of the expansion coefficients are needed to confirm these conclusions.

Finally, a few points concerning the dichroic asymmetry of the $2p_{1/2}$ peak should be noted. The model predicts that the poor energy resolution of the experiments should remove the explicit β-dependence of the ratio of peak-to-peak asymmetries at the $2p_{1/2}$ and $2p_{3/2}$ features. This prediction is tested in table 1, where the ratio of the peak-to-peak asymmetries in the $2p_{1/2}$ and $2p_{3/2}$ features are compared for emission along high-symmetry directions. Along these directions, the expansion coefficients drop out, and only the explicit angular dependence remains. The calculated ratios show that the broadening has indeed removed the explicit angular dependence. The experimental ratios for the different geometries are also indistinguishable within error and agree well with the model calculation. These results are consistent with various angle-integrated calculations [14, 16, 31] of magnetic circular dichroism in photoemission, which give a ratio [35] of −0.32 to −0.53.

In the lower-symmetry situation of emission along a general direction in a mirror plane, the $2p_{1/2}$ data in figure 7 confirm the departure from the model calculation based on photoelectron states of atomic symmetry. Given the scatter of the data, the curvature of the plot of the $2p_{1/2}$ peak asymmetry is difficult to quantify. It is not possible to judge unambiguously whether or not the ratio of the asymmetries at the $2p_{1/2}$ and $2p_{3/2}$ peaks remains constant as β is varied. The ratio calculated from the data in figure 7 remains within the range -0.40 ± 0.10. If this ratio is independent of β, it would indicate that the expansion coefficients B_m are similar for photoelectrons produced by transitions from either the $2p_{1/2}$ or $2p_{3/2}$ level. This need not be the case.

5. Conclusions

There is an angular dependence of the magnitude of the MCD in angle-resolved photoemission from iron core levels. New and additional data support the earlier suggestion [18] that the dichroic asymmetry depends on geometric selection through the relative orientations of the light wavevector q, the magnetization M, and the photoelectron wavevector k. Furthermore, a study of the angular dependence of the dichroic asymmetry in a mirror plane, now shows that it is also linked to the sample through the absolute orientation of k in the crystalline axes.

These angular dependences were not appreciated earlier, and calculations of the dichroic asymmetry were based on angle-integrated absorption models and/or models

which used an oriented, single atom. A simple, angle-resolved model can explain the important aspects of the angular dependence by taking into account the symmetry of the photoelectron states and their coupling to the detector. It is necessary to distinguish two situations. For emission along high-symmetry directions (3 or more mirror planes) the model gives quantitative predictions without detailed calculation of the crystalline wavefunctions. These predictions are in excellent agreement with observed relative magnitudes of the peak-to-peak dichroic asymmetry in the $2p_{3/2}$ peak in different experimental geometries, and with the relative ratio of the asymmetry in the $2p_{1/2}$ and $2p_{3/2}$ peaks in these same geometries. It also explains why the asymmetry does *not* disappear when $q \cdot M = 0$ for angle-resolved experiments, but *does* disappear in angle-integrated experiments. However, experiments in this geometry cannot distinguish whether the photoelectron states may be treated as states of an oriented atom, or must conform to the symmetry of the crystal.

For emission in the lower-symmetry situation of a single mirror plane, the use of photoelectron states of atomic or crystalline symmetry lead to different model predictions. The use of states of atomic symmetry predicts that the dependence of the dichroic asymmetry on the emission angle is given by the same function as for emission along high-symmetry directions. The data clearly contradict this prediction. For states of crystalline symmetry, it is not possible to make quantitative predictions without full-scale calculations of the wavefunctions. However, the model makes the qualitative prediction that the dichroic asymmetry in the 2p peaks is reduced symmetrically in emission angle as it moves away from a high-symmetry direction. Such an angular dependence is seen experimentally.

It is hoped that this investigation will prompt explicit calculations of the photoelectron wavefunctions to evaluate the angular dependence of MCD in angle-resolved core-level photoemission. It seems that such a calculation must address the effects of crystal structure on the photoelectron wavefunction, and cannot rely on a model based on an oriented, single atom.

Acknowledgments

DV wishes to acknowledge partial support by the Natural Sciences and Engineering Research Council of Canada, and the Deutsche Forschungsgemeinschaft, which has allowed him to participate in these experiments. This work was supported by the Bundesminister für Forschung und Technologie under contract 05 413 AXI, TP 06.

References

[1] Erskine J L and Stern E A 1975 *Phys. Rev.* B **12** 5016
[2] van der Laan G, Thole B T, Sawatzky G A, Goedkoop J B, Fuggle J C, Esteva J-M, Karnatak R, Remeika J P and Dabkowska H A 1986 *Phys. Rev.* B **34** 6529
[3] Schütz G, Wagner W, Wilhelm W, Kienle P, Frahm R and Materlik G 1987 *Phys. Rev. Lett.* **58** 737
[4] Chen C T, Sette F, Ma Y and Modesti S 1990 *Phys. Rev.* B **43** 7262
[5] Thole B T, van der Laan G and Sawatzky G A 1985 *Phys. Rev. Lett.* **55** 2086
[6] Goedkoop J B, Thole B T, van der Laan G, Sawatzky G A, de Groot F M F and Fuggle J C 1988 *Phys. Rev.* B **37** 2086
[7] Chen C T, Smith N V and Sette F 1991 *Phys. Rev.* B **43** 6785
[8] Jo T and Sawatzky G A 1991 *Phys. Rev.* B **43** 8771
[9] Ebert H, Strange P and Gyorffy B L 1988 *Z. Phys.* B **73** 77

[10] Brouder C and Hikam M 1991 *Phys. Rev.* B **43** 3809
[11] Carra P, Harmon B N, Thole B T, Altarelli M and Sawatzky G A 1991 *Phys. Rev. Lett.* **66** 2495
[12] Baumgarten L, Schneider C M, Petersen H, Schäfers F and Kirschner J 1990 *Phys. Rev. Lett.* **65** 492
[13] Baumgarten L, Yumoto S, Schneider C M, Kirschner J, Petersen H and Schäfers F 1990 *BESSY* Jahresbericht, p 191
[14] Ebert H, Baumgarten L, Schneider C M and Kirschner J 1991 *Phys. Rev.* B **44** 4406
[15] Ebert H 1991 *J. Phys.: Condens. Matter* **1** 9111
[16] van der Laan G 1991 *Phys. Rev. Lett.* **66** 2527
van der Laan G 1991 *J. Phys.: Condens. Matter* **3** 1015
[17] Thole B T and van der Laan G 1991 *Phys. Rev. Lett.* **67** 3306
[18] Schneider C M, Venus D and Kirschner J 1992 *Phys. Rev.* B **45** 5041
[19] Petersen H 1986 *Nucl. Instrum. Methods* A **246** 260
[20] Petersen H 1992 private communication
[21] Carra P and Altarelli M 1990 *Phys. Rev. Lett.* **64** 1286
[22] Oepen H-P, Hünlich K and Kirschner J 1986 *Phys. Rev. Lett.* **56** 496
[23] Feder R 1985 *Polarized Electrons in Surface Physics* ed R Feder (Singapore: World Scientific)
[24] Even if the effect of the different backgrounds is not taken into account, the variations of $\pm 1.5\%$ in the asymmetries of the Auger electrons do not show the characteristic spectral shape of MCD. This may be contrasted with the peak-to-peak asymmetry of similar magnitude in the $2p_{1/2}$ feature in figure 2, which shows a clear minus/plus feature correlated to the plus/minus feature at the $2p_{3/2}$ peak.
[25] Magnetic deflection effects scale as $1/\sqrt{E}$, so the Auger data are about 2 times less sensitive to magnetic deflection than the photoemission data. However, given the smaller background in the Auger spectrum, it is a more sensitive test of asymmetries caused by magnetic deflection.
[26] Rose M E 1957 *Elementary Theory of Angular Momentum* (New York: Wiley)
[27] For the symmetry arguments which follow, 'diffracted photoelectron' states would suffice equally.
[28] Hermanson J 1977 *Solid State Commun.* **22** 9
[29] Fuggle J C and Alvarado S F 1980 *Phys. Rev.* A **22** 1615
[30] Bradley C J and Cracknell A P 1972 *The Mathematical Theory of Symmetry in Solids* (Oxford: Clarendon)
[31] Imada S and Jo T 1991 *J. Phys. Soc. Japan* **60** 2843
[32] This is seen in the well-known expansion of a plane wave into spherical harmonics, which is restricted to $m = 0$ terms.
[33] Jackson J D 1975 *Classical Electrodynamics* 2nd edn (New York: Wiley) p 277
[34] Gradmann U and Alvarado S F 1985 *Polarized Electrons in Surface Physics* ed R Feder (Singapore: World Scientific) ch 7
[35] A clear distinction should be made between these ratios and those in measurements of absorption at L edges in iron. In the latter case, the asymmetry has a single sign for each peak, and $A(2p_{1/2})/A(2p_{3/2}) \approx -2.0$. See [3, 5, 7].